Observation of Interlayer Excitons in Monolayer $MoSe_2 - WSe_2$ Heterostructures on BN substrate

Alice Huang,[1,2] Essance Ray,[3] Pasqual Rivera,[4] Kyle Seyler,[4] Eric Wong,[4] Paul Nyugen,[4] Genevieve Clark,[5] and Xiaodong Xu[4,5]

[1)] *Department of Physics and Astronomy, Rutgers University, Piscataway, NJ*
[2)] *Institute for Nuclear Theory REU, University of Washington, Seattle, WA*
[3)] *Clean Energy Institute Undergraduate Fellowship, University of Washington, Seattle, WA*
[4)] *Department of Physics, University of Washington, Seattle, WA*
[5)] *Department of Materials Science and Engineering, University of Washington, Seattle, WA*

(Dated: August 29, 2015)

Interlayer excitons have previously been observed in monolayer MX_2 heterostructures exhibiting type II band alignment. Specifically, interlayer excitons in $MoSe_2 - WSe_2$ heterostructures have been thoroughly characterized with photoluminescence (PL) and photoluminescence excitation spectroscopy (PLE). However electrical control of the interlayer exciton exhibits PL intensity dependence that is inconsistent with the dipole and electric field model – possibly owing to carrier charge effects – and requires further elucidation. The addition of BN substrate, which has been shown to (1) smooth the surface and (2) reduce carrier charge inhomogeneity of graphene devices, presents itself as a potential solution. In this preliminary study, we fabricated an $MoSe_2 - WSe_2$ heterostructure on BN substrate. Photoluminescence (PL) measurements on the device confirm the presence of interlayer excitons at approximately 1.40 eV, consistent with $MoSe_2 - WSe_2$ heterostructures. Furthermore, the PL characterization reveals unreported spectral features for both the interlayer and intralayer excitons.

I. INTRODUCTION

With more than ten thousand papers published each year, graphene is one of the most intensely pursued research topics in condensed matter. In the past half-decade, the study of two-dimensional electron systems has extended to other monolayer atomic crystals such as transition metal dichalcogenides (TMDs) as well as van der Waals heterostructures[1].

Monolayer TMDs (chemical formula: MX_2) are three atoms thick with a single layer of transition-metal atoms (tungsten W or molybdenum Mo) sandwiched between layers of chalcogens (sulfur S or selenium Se) [Figure 1a]. While monolayer TMDs share the same honeycomb hexagonal lattice as graphene, TMDs are true semiconductors, exhibiting a direct bandgap at the monolayer limit[2].

Meanwhile, the stacking of two-dimensional materials to create novel heterostructures held together by van der Waals forces [Figure 1b] has proven to be a versatile platform for studying optoelectronic phenomena at the two-dimensional limit. In particular, TMD heterostructures have atomically sharp interfaces with no interdiffusion of atoms; thus indicating the potential for control of individual layer components[3]. In this preliminary study, we focus on the excitonic response of TMD $MoSe_2 - WSe_2$ heterostructure on BN. Because TMDs have a high Coulomb binding energy of several hundred meV (much greater than typical semiconductors and nearly two orders greater than GaAs quantum wells), these semiconductors demonstrate high excitonic response that is electrically tunable even at room temperature[4].

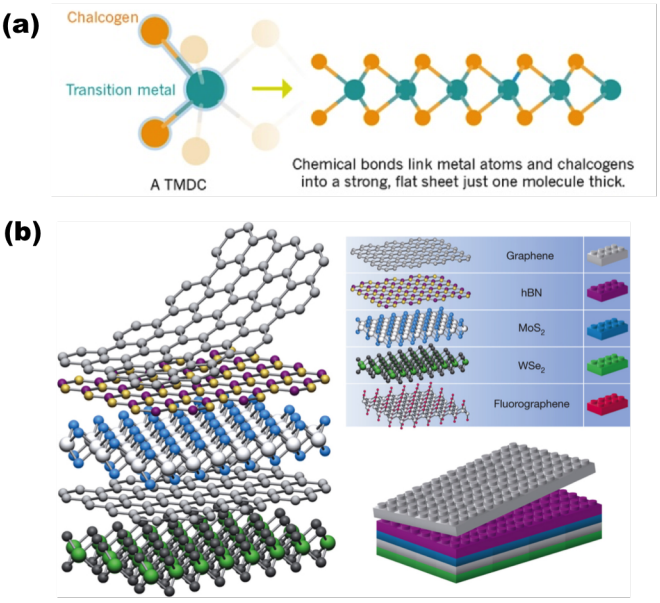

FIG. 1. **MX_2's and van der Waals Heterostructures** (a) Monolayer TMDs consist of a layer of transition-metal atoms sandwiched between chalcogens coordinated in a trigonal prismatic structure[2]; (b) Building van der Waals heterostructures can be likened to atomic-scale lego[1]

II. EXCITONS IN 2D MATERIALS: AN EXPERIMENTAL OVERVIEW

A. Introduction to Excitonic Physics in Monolayer MX_2[4,5]

Absorption of a photon with energy surpassing the material's bandgap: (1) excites the valence band electron in the conduction band, and (2) creates a 'hole' in the valence band where the electron once was. Given sufficient Coulomb binding energy, the electron and hole bind together to form an exciton, a quasi-particle analogous to the hydrogen atom[6,7]. Conversely, when the photo-excited electron relaxes and recombines with the hole, a photon is emitted. This is the process behind the photoluminescence (PL) measurements conducted in this study.

Monolayer MX_2's have direct bandgaps, which unlike indirect bandgaps don't necessitate phonon assisted transitions and allow for the observation of PL. Characterization of MoS_2 as a function of layer number with PL, optical absorption, and photoconductivity measurements demonstrate a crossover from indirect to direct bandgap at the 2D monolayer limit[5]. The PL spectra of monolayer MoS_2 shows one emission peak centered at 1.90 eV [Figure 2a]. This monolayer emission peak exactly matches the lower resonance peak of the absorption spectrum in both position and width [Figure 2b]. This absorption and emission of photons of the same wavelength or energy implies direct-gap luminescence. Furthermore, the PL of the indirect bandgap as a function of decreasing layer number experiences a shift from 1.29 eV to 1.90 eV while the direct bandgap only increases by 0.1 eV, indicating a crossover from an indirect to a direct bandgap [Figure 2c]. Perhaps most revealingly, the PL quantum yield (QY) for monolayer samples is dramatically brighter than its few sample counterparts. In fact without normalization, the QY for monolayer samples is two to three orders of magnitude greater than that of its bilayer counterparts [Figure 2a].

Due to the high Coulomb binding energy of MX_2's, the neutral exciton X^0 can bind with an additional electron or hole to become a trion, a charged three-body particle X^- and X^+ respectively. Gate dependent PL measurements demonstrate the electric tunability of these excitons in $MoSe_2$[4]. When a vertical gate bias is applied to the monolayer semiconductor, PL as a function of back-gate voltage V_g shows distinct spectral peaks for X^0, X^+, and X^- excitons [Figure 3a]. At zero V_g, neutral excitons X^0 are observed. With the application of negative V_g bias, the the sample becomes increasingly p-doped (increasingly hole dominated) and X^+ excitons prevail [Figure 3b]. Likewise with the application of positive V_g bias, the sample becomes increasingly n-doped (increasingly electron dominated) and X^- excitons prevail. The spectral peaks for the two trions are analogous in energy and intensity, indicating electrons and holes have the same effective mass.

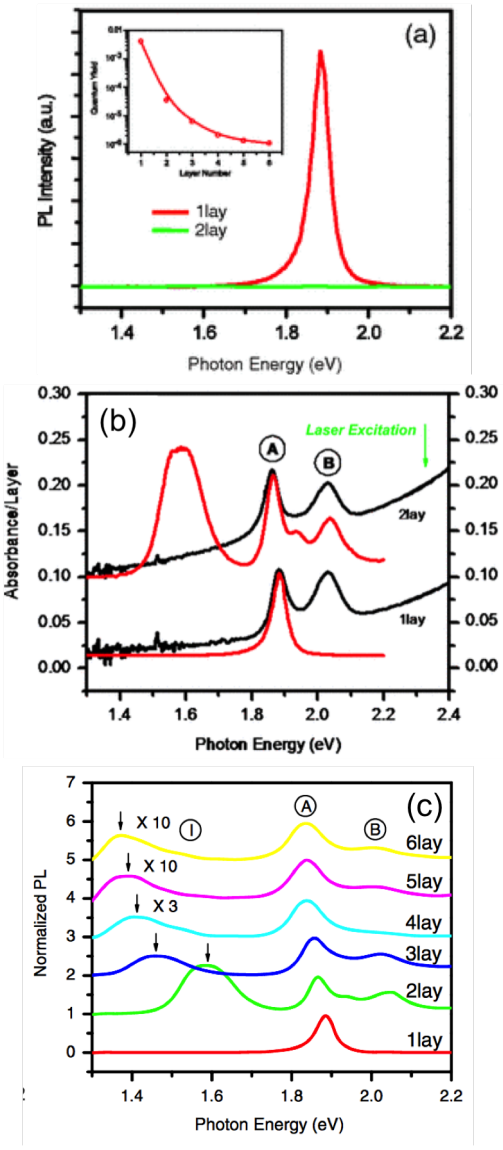

FIG. 2. **PL and absorption characterization of MoS_2** (a) PL QY of monolayer MoS_2 samples are dramatically brighter than its bilayer counterparts, indicating a crossover to direct band luminescence at the 2D limit; (b) The monolayer PL peak exactly matches the width and height of the lower monolayer absorption peak, implying direct band luminescence; (c) Normalized PL as a function of layer number indicates a crossover from indirect to direct bandgap[5]

The combination of direct band luminescence and electric tunability make monolayer MX_2's an ideal material for exploring excitonic physics at the 2D limit.

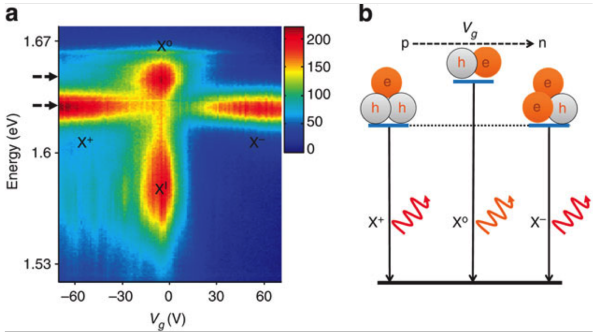

FIG. 3. **Gate control of excitons** (a) $MoSe_2$ PL as a function of back-gate voltage; (b) Cartoon illustration of gate-dependent trion and exciton transitions[4]

B. Observation of Interlayer Excitons in Monolayer $MoSe_2 - WSe_2$ Heterostructures[8]

Because different TMD monolayers have varying intrinsic properties, the stacking of different TMD monolayers may result in physical phenomena not present in their individual counterparts. In particular, interlayer excitons have previously been observed in monolayer $MoSe_2 - WSe_2$ heterostructures. This is owing to the heterostructure's staggered type II band alignment formed by the combination of individual TMD bandgaps and work functions. Due to the strong TMD exciton binding energy, electrons and holes are localized within a monolayer and interlayer excitonic states may be realized. While the photo-excited electron relaxes to the conduction band of $MoSe_2$, the photo-excited hole relaxes to the valence band of WSe_2. In this heterojunction, $MoSe_2$ is n-doped and WSe_2 is p-doped. The resulting Coulomb attraction binds the two together to form an interlayer exciton [Figure 4a].

Room temperature and low temperature PL characterization of the heterostructure exhibits an interlayer exciton peak, distinct from the monolayer intralayer exciton peaks of $MoSe_2$ and WSe_2 [Figure 4b]. In the heterostructure region, the intralayer peaks occur at the same energy positions as the spectral peaks for the monolayers alone; thus demonstrating that intralayer excitons are preserved in the heterostructure. Two-dimensional spatial mapping of spectrally integrated PL intensity confirms that the interlayer spectral feature is localized in the heterostructure region, verifying the presence of interlayer excitons.

In attempt to gate control the interlayer exciton, a vertical gate bias was applied to the heterostructure. With the application of negative back-gate voltage, one expects reduced band offset of the p-n junction and increased potential energy of the exciton, $U = -p * E$. This was demonstrated by the blue shift in PL energy as a function of back-gate voltage [Figure 5b]. Additionally due to the heterostructure's staggered type II band alignment, one expects a permanent dipole pointing from

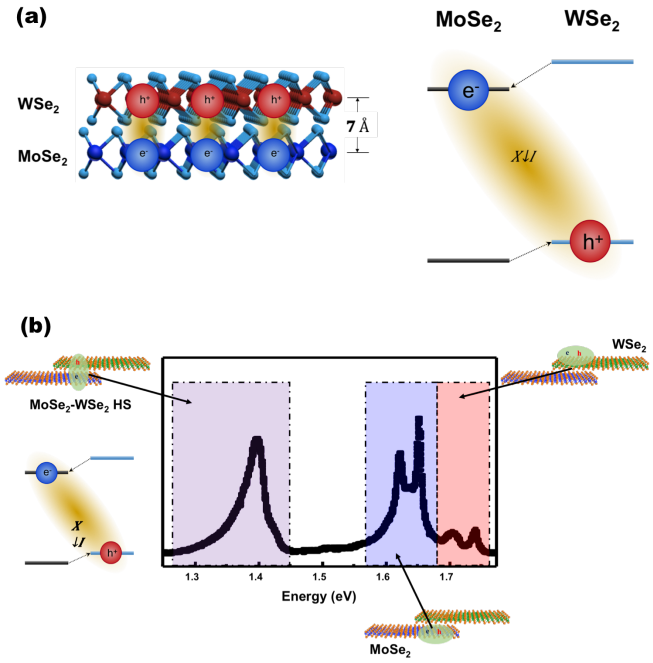

FIG. 4. **Observation of interlayer exciton in $MoSe_2 - WSe_2$ HS** (a) An interlayer exciton forms in $MoSe_2 - WSe_2$ heterostructures due to type II heterojunction between $MoSe_2$ and WSe_2; (b) PL measurements reveal an interlayer exciton peak, distinct from the monolayer intralayer exciton peaks (Images courtesy of Pasqual Rivera and Kyle Seyler)

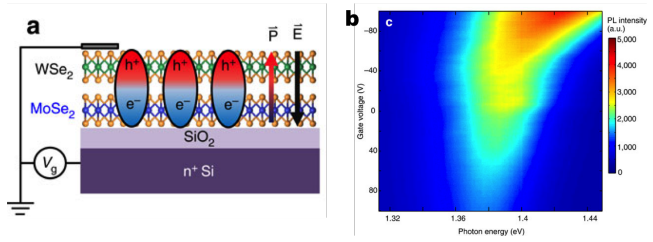

FIG. 5. **Electrical control of the interlayer exciton** (a) Cartoon illustration of application of vertical gate bias onto the $MoSe_2 - WSe_2$ heterostructure and its resulting dipole alignment (b) PL measurements as a function of applied voltage; with the application of negative V_g, the PL intensity blue shifts due to reduced type II band offset[8]

$MoSe_2$ to WSe_2 [Figure 5a]. While this was consistent for $MoSe_2 - WSe_2$ devices, when the stacking order of $MoSe_2$ and WSe_2 monolayers was reversed the PL intensity with respect to applied voltage did not change accordingly [Figure 5b]. This anomaly was attributed to charge carrier doping.

The addition of a dielectric substrate would potentially elucidate the anomaly of PL intensity dependence. It is also expected to clarify the width of the interlayer

PL peak. Specifically, why is the PL peak of the interlayer exciton two to three times greater than its intralayer counterparts? In both instances, this is perhaps due to the issue of substrate inhomogenity – both in surface charge traps and flatness.

C. BN Substrate for Ultra-Flat High Quality Electronics[9,10]

Hexagonal boron nitride (h-BN) has shown to be an appealing alternative to SiO_2 substrate for ultra-flat high quality electronics. Atomic force microscopy measurements that map the morphology of a sample show graphene is smoothed by h-BN [Figure 6a]. The height distribution for h-BN is nearly identical to graphene on h-BN, indicating that graphene adheres to h-BN. In comparison the distribution width for SiO_2 is three times as large.

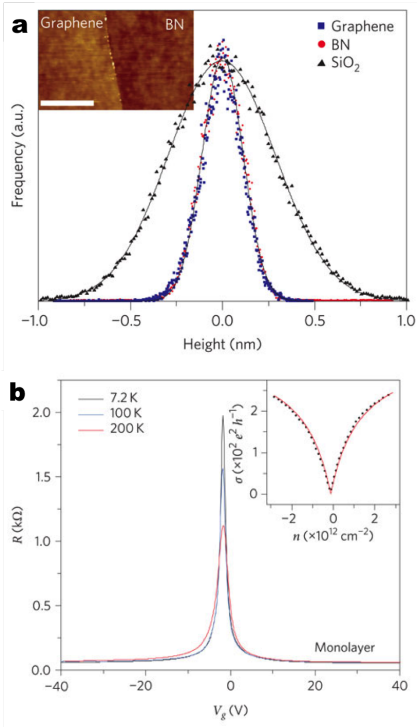

FIG. 6. **BN substrate atomic force spectroscopy and transport properties** (a) Histogram of roughness of graphene on h-BN substrate extrapolated from AFM measurements (b) Resistivity of graphene on h-BN as a function of back-gate voltage[9]

In addition, h-BN inert and free of dangling bonds and surface charge traps. For graphene on h-BN, the resistivity peak as a function of backgate voltage (otherwise the charge neutrality point) occurs close to $V_g = 0$ [Figure 6b]. This implies h-BN is already charge neutral without the application of an external voltage. From the width of this resistivity peak, the carrier inhomogeneity was determined to be $\delta_n < 7 * 10^{10}$ cm^{-2}, three times better than graphene samples on SiO_2.

III. PROJECT OBJECTIVE, HYPOTHESIS, QUESTIONS

The objective of this project was to fabricate and transfer a $MoSe_2 - WSe_2$ heterostructure onto BN substrate. We hypothesize that the BN substrate will (1) smooth the heterostructure surface and (2) reduce the heterostructure carrier charge effects. Questions we hope to elucidate: will smoothing of the surface change the band structure and the excitonic behavior of the heterostructure? Also, will reducing charge carrier effects result in behavior that is consistent with the dipole and electric field model?

IV. SAMPLE FABRICATION

A. Mechanical Exfoliation

$MoSe_2$ and WSe_2 monolayers and BN substrate were fabricated by mechanical exfoliation (via the scotch tape method) onto SiO_2 chips. Each SiO_2 chip was manually searched under an optical microscope. Thin film interference allowed monolayers (or the desired sample) to be identified based on color contrast to the SiO_2 chip[11]. $MoSe_2$ and WSe_2 monolayers were fabricated on 300 nm thick SiO_2 and assumed a plum color [Figure 7]. Meanwhile BN was fabricated on 90 nm thick SiO_2 and assumed a slate blue color. Each sample piece was approximately 10 μm by 10 μm.

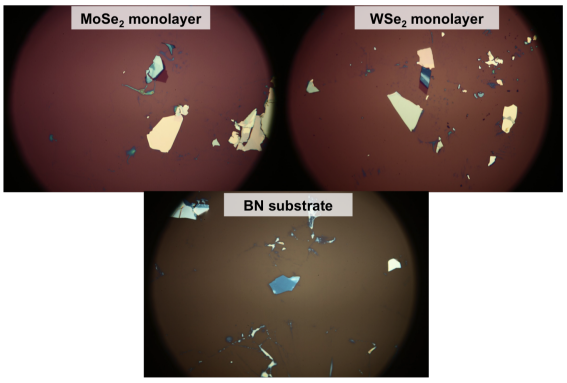

FIG. 7. **Samples under optical microscope (100x magnification)** $MoSe_2$ monolayer on 300 nm SiO_2, WSe_2 monolayer on 300 nm SiO_2, and BN substrate on 90 nm SiO_2

B. Atomic Force Spectroscopy

After the desired sample pieces were isolated, the sample morphology was mapped under atomic force spectroscopy (AFM) to determine sample cleanliness. The AFM utilizes a probe which oscillates at resonant frequency. As the probe draws closer to the surface, the sample is subjected to electrostatic forces – attractive van der Waals forces and repulsive Coulomb force – altering the probe frequency[12]. The sample's morphology can subsequently be extracted.

All samples were clean under the AFM as demonstrated by the samples' smooth and homogeneous surfaces [Figure 8]. In contrast, a sample with tape residue would generally exhibit spotting that is more elevated than the rest of the sample.

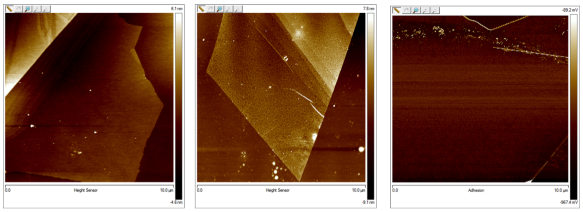

FIG. 8. **AFM characterization of samples in Figure 7** demonstrate the cleanliness of the samples

C. Cleaning

Due to the inherent difficulty of finding MX_2 monolayers that were sufficiently clean, we conducted a simple experiment to determine the best method for cleaning MX_2 monolayers. In total, ten samples were characterized with the AFM and/or optical microscope.

The resulting recommended monolayer MX_2 cleaning procedure is as follows.

1. Fifteen minutes in tetrahydrofuran (THF) (boiling point: 66°C) at 50°C with a glass cover
2. Immediately wash off with isopropanol (IPA) and dry with nitrogen

While THF was successful in cleaning the samples, acetone was not. In the first characterization, the AFM reveals a significant improvement in cleanliness after a THF bath but no significant improvement after an acetone bath [Figure 9]. In the second characterization, where the order of chemical baths was reversed – the sample was bathed in THF followed by acetone – the acetone bath deposited residue on the THF cleaned monolayer [Figure 10].

Furthermore, the time of bath in THF was reduced from one hour to fifteen minutes. In one characterization, there was no significant improvement from a fifteen minute of bath THF to a thirty minute bath of THF.

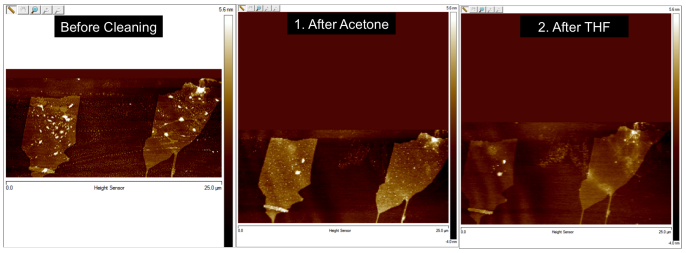

FIG. 9. **AFM characterization of monolayer cleaned in acetone bath followed by THF bath** shows a significant improvement in cleanliness after a THF bath but not an acetone bath

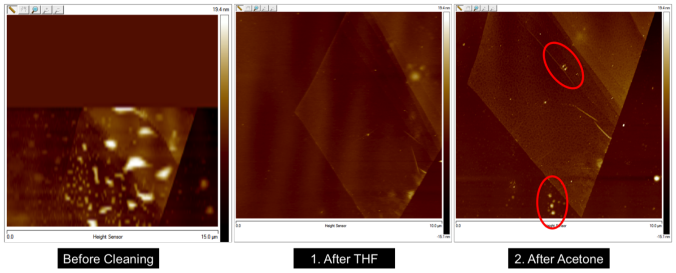

FIG. 10. **AFM characterization of monolayer cleaned in THF bath followed by acetone bath** shows increased residue following the acetone bath

Another characterization showed that the residue on the monolayer increased after more than fifteen minutes in THF [Figure 11].

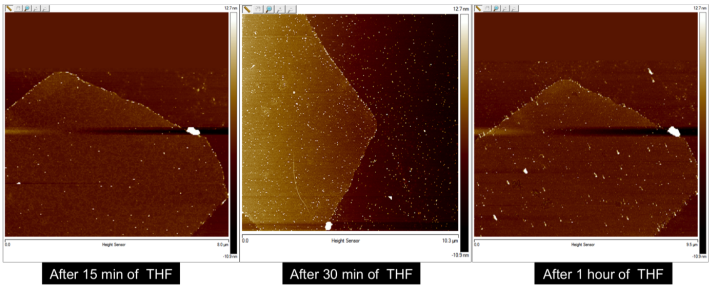

FIG. 11. **AFM characterization of monolayer in 15 min, 30 min, and 1 hour in THF** reveals the monolayer is cleanest after 15 min in THF

D. Heterostructure Transfer Technique[13]

The transfer technique for fabricating heterostructures can be summarized in the following five steps.

1. A polymer stamp consisting of PDMS covered with PC film is melted upon the desired sample in the desired orientation.

2. The set-up is subsequently cooled. The sample mount contracts, allowing the sample to lift off of the SiO_2 chip onto the stamp.

3. The previous two steps are repeated for the desired heterostructure stack.

4. For the last transfer, rather than picking up the final layer, the PC layer with the heterostructure is melted onto the SiO_2 chip.

5. The SiO_2 chip is washed with chloroform to clean off the PC film.

V. DATA COLLECTION AND RESULTS

A. $MoSe_2 - WSe_2 - BN$ Device

Following the fabrication procedure delineated above, a $MoSe_2 - WSe_2 - BN$ device was fabricated [Figure 12].

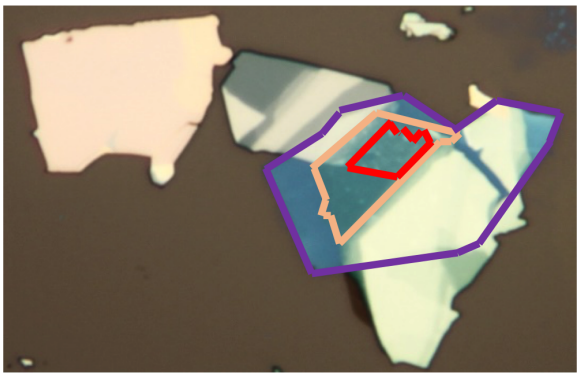

FIG. 12. **$MoSe_2 - WSe_2 - BN$ Device**: the $MoSe_2$ monolayer is outlined in yellow, the WSe_2 monolayer is outlined in red, and the BN substrate is outlined purple

B. Photoluminescence Characterization

The $MoSe_2 - WSe_2 - BN$ device was first characterized by its optical response at room temperature (300 K) and low temperature (4 K). The sample was excited under a continuous wave (CW) laser at 2.33 eV, and the PL from the sample was subsequently measured. The PL from the sample was spectrally dispersed through a 0.5 monochromator before detection by a charge-coupled device (CCD).

Room temperature PL characterization exhibits three distinct spectral features at 1.35 eV, 1.57 eV, and 1.65 eV [Figure 13a]. The emission of 1.35 eV corresponds to the PL measured from the heterostructure region and is attributed to the interlayer exciton. Likewise the 1.57 eV and 1.65 eV emissions correspond to the PL measured from the individual monolayers and can be attributed the to the intralayer excitons from $MoSe_2$ and WSe_2, respectively. Moreover, these energy emission values match the energy band-gap values predicted by the type II band alignment model [Figure 13b]. These spectral features of the $MoSe_2 - WSe_2 - BN$ device are consistent with PL measurements of $MoSe_2 - WSe_2$ heterostructures at room temperature.

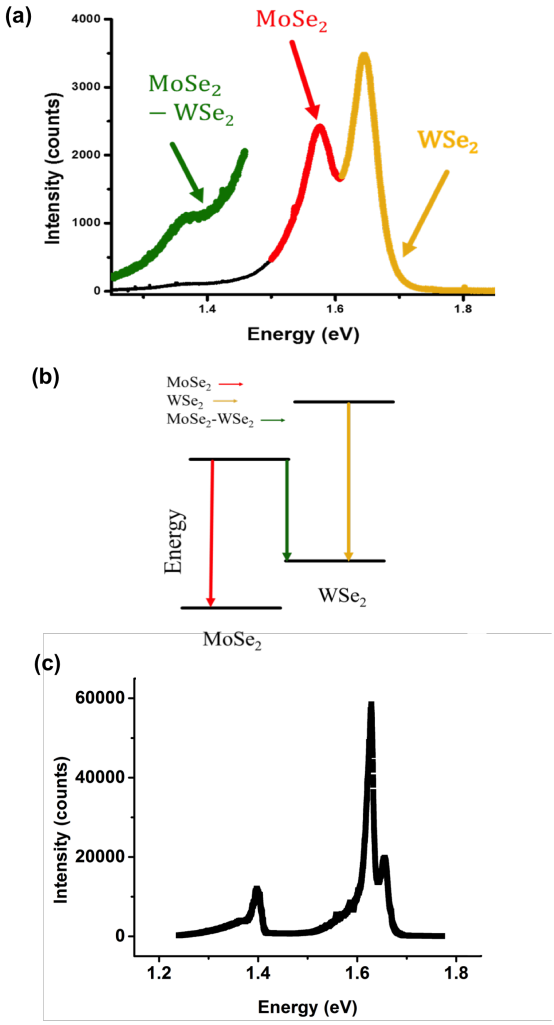

FIG. 13. **Intralayer and interlayer excitons of a monolayer $MoSe_2 - WSe_2$ heterostructure on BN substrate** (a)Room temperature (300 K) PL characterization (excitation energy of 2.33 eV with 5 second integration time under 5 μW) shows an interlayer exciton peak distinct from the intralayer $MoSe_2$ exciton peak and intralayer WSe_2 exciton peak. The interlayer exciton peak is displayed 10x on the graph. (b) Illustration of the $MoSe_2 - WSe_2$ type II band alignment and the corresponding energy emissions. (c) Low temperature (4K) PL characterization (excitation energy of 2.33 eV with 2 second integration time under 100 W) exhibits an interlayer exciton peak, an $MoSe_2$ exciton peak, and an $MoSe_2$ trion peak.

Low temperature (4 K) PL characterization exhibits three dominant spectral features at 1.40 eV, 1.63 eV, and 1.65 eV [Figure 13c]. The 1.40 eV emission corresponds to the interlayer exciton. The width of this peak is approximately 30 meV, nearly 10 meV less than the most narrow interlayer $MoSe_2 - WSe_2$ exciton peak observed. Meanwhile the 1.63 eV emission corresponds to the intralayer exciton from the $MoSe_2$. The third spectral emission at 1.65 eV occurs at the tail end of the $MoSe_2$ intralayer exciton, likely an intralayer trion from the monolayer $MoSe_2$. This additional trion is unreported in $MoSe_2 - WSe_2$ heterostructures.

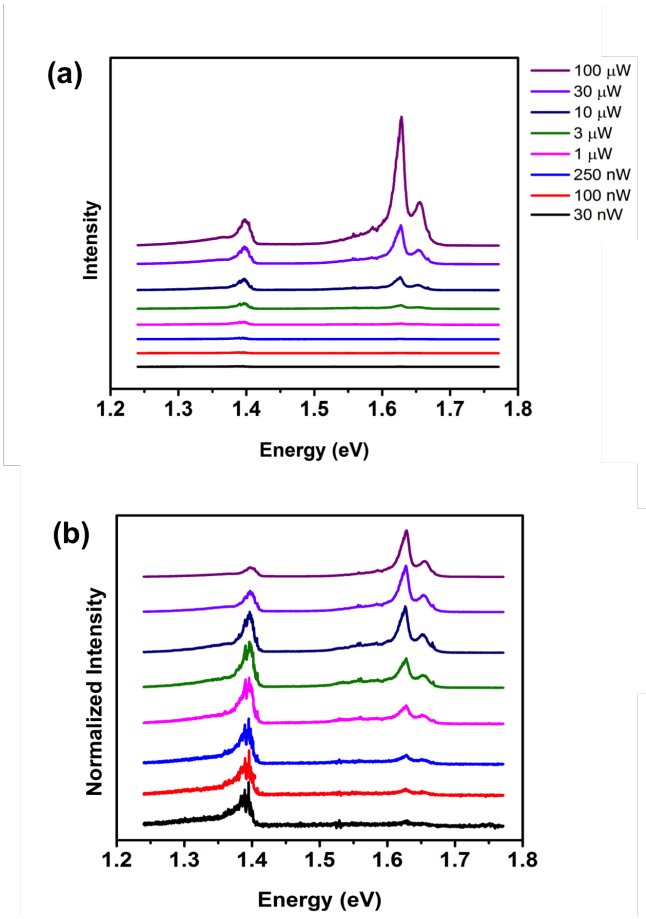

FIG. 14. **Power dependent PL characterization** (a) Power dependent PL characterization (excitation energy of 2.33 eV with 2 second integration time under power ranging from 30 nW to 100 μW) shows the evolution of PL as a function of power. (b) Normalization of power dependent PL shows a defect related doublet feature in the interlayer exciton spectral emission, which saturates with increasing power.

Following room temperature and low temperature PL measurements, the device was characterized by power dependent PL. The power was manually adjusted with an attenuator and power meter, and PL from the device was subsequently measured. The power was increased by about one-third order of magnitude ranging from 30 nW to 100 μW (30 nW, 100 nW, 250 nW, 1 μW, 3 μW, 10 μW, 30 μW, 100 μW) for a total of eight PL measurements. The sample was excited with a continuous wave (CW) laser at 2.33 eV and PL measurements were obtained with 2 second integration time.

With increased power, the PL spectral features described in the low temperature PL characterization become more pronounced [Figure 14a]. Normalization of the PL intensity reveals the interlayer exciton saturates with increasing power. As the interlayer exciton saturates, the $MoSe_2$ intralayer exciton peaks become more pronounced. Also previously unreported, the normalized graph shows a defect-related doublet feature in the interlayer exciton peak that diminishes with increasing power.

VI. DISCUSSION

While room temperature PL of a $MoSe_2 - WSe_2 - BN$ exhibits exciton peaks consistent with the $MoSe_2 - WSe_2$ heterostructure spectrum, low temperature PL reveals unreported features in both the interlayer and intralayer excitons. This includes an extremely narrow heterostructure peak, a doublet feature in the heterostructure peak, and an $MoSe_2$ trion peak. Physical interpretation of these spectral features have yet to be developed and tested.

The fabrication and testing of additional $MoSe_2 - WSe_2 - BN$ heterostructures would potentially elucidate these PL spectral features. Improvement in device fabrication includes performing second harmonic generation on individual monolayers to determine the polarization axes of the sample in order to fabricate a $MoSe_2 - WSe_2$ device with crystal alignment. Moreover, we would like to fabricate heterostructures with reversed stacking order – $WSe_2 - MoSe_2 - BN$ – to investigate the role of stacking order in interlayer excitonic states.

Future testing of the $MoSe_2 - WSe_2 - BN$ heterostructure includes but is not limited to temperature dependent PL, electrical control of the interlayer exciton, and valley polarization of interlayer and intralayer excitons. Of particular interest is to measure the lifetime of the interlayer exciton and compare to lifetime measurements of interlayer excitons from $MoSe_2 - WSe_2$ heterostructures. It would also be of particular interest to conduct STM and STS measurements on the $MoSe_2 - WSe_2 - BN$ heterostructure to examine if the $MoSe_2 - WSe_2$ heterostructure is truly flat on the BN substrate and to identify the origin of the carrier doping.

VII. ACKNOWLEDGEMENTS

Thank you to Xiaodong Xu for this wonderful summer lab experience. Special thanks to Pasqual Rivera and Kyle Seyler for being outstanding mentors. Thank you to Essance Ray, Eric Wong, Paul Nguyen, Genevieve Clark, Jason Ross, Sanfeng Wu, Harold Cai, John

Schaibley, Ding Zhong, Jae Hwan Chu, Nathan Wilson, and Bevin Huang who assisted me in lab on a daily basis. Thank you to Ron Musgrave for the machine shop lessons. Thank you to the REU coordinators and the NSF. Finally, thank you to my REU cohort for making this such a memorable experience.

---

[1] A. K. Geim and I. V. Grigorieva and. Van der waals heterostructures. Nature 499:7459, 07 2013.

[2] Elizabeth Gibney. The super materials that could trump graphene. Nature News 522:7556, 06 2015.

[3] Hui Fang, Corsin Battaglia, Carlo Carraro, Slavomir Nemsak, Burak Ozdol, Jeong Seuk Kang, Hans A. Bechtel, Sujay B. Desai, Florian Kronast, Ahmet A. Unal, Giuseppina Conti, Catherine Conlon, Gunnar K. Palsson, Michael C. Martin, Andrew M. Minor, Charles S. Fadley, Eli Yablonovitch, Roya Maboudian, and Ali Javey. Strong interlayer coupling in van der waals heterostructures built from single-layer chalcogenides. 03 2014.

[4] Jason S. Ross, Sanfeng Wu, Hongyi Yu, Nirmal J. Ghimire, Aaron M. Jones, Grant Aivazian, Jiaqiang Yan, David G. Mandrus, Di Xiao, Wang Yao, and Xiaodong Xu. Electrical control of neutral and charged excitons in a monolayer semiconductor. *Nat Commun*, 4:1474, 02 2013.

[5] Kin Fai Mak, Changgu Lee, James Hone, Jie Shan, and Tony F. Heinz. Atomically thin mos_2: A new direct-gap semiconductor. *Phys. Rev. Lett.*, 105:136805, Sep 2010.

[6] Chris Dunleavy David Brook Knowles, Kevin. Introduction to semiconductors. DoITPoMS, University of Cambridge, 08 2007.

[7] David A. B. Miller. Optical physics of quantum wells.

[8] Pasqual Rivera, John R. Schaibley, Aaron M. Jones, Jason S. Ross, Sanfeng Wu, Grant Aivazian, Philip Klement, Kyle Seyler, Genevieve Clark, Nirmal J. Ghimire, Jiaqiang Yan, D. G. Mandrus, Wang Yao, and Xiaodong Xu. Observation of long-lived interlayer excitons in monolayer mose2–wse2 heterostructures. *Nat Commun*, 6, 02 2015.

[9] DeanC. R., YoungA. F., MericI., LeeC., WangL., SorgenfreiS., WatanabeK., TaniguchiT., KimP., ShepardK. L., and HoneJ. Boron nitride substrates for high-quality graphene electronics. *Nat Nano*, 5(10):722–726, 10 2010.

[10] Jiamin Xue, Javier Sanchez-Yamagishi, Danny Bulmash, Philippe Jacquod, Aparna Deshpande, K. Watanabe, T. Taniguchi, Pablo Jarillo-Herrero, and Brian J. LeRoy. Scanning tunnelling microscopy and spectroscopy of ultra-flat graphene on hexagonal boron nitride. *Nat Mater*, 10(4):282–285, 04 2011.

[11] P. Blake, K. S. Novoselov, A. H. Castro Neto, D. Jiang, R. Yang, T. J. Booth, A. K. Geim, and E. W. Hill. Making graphene visible. 05 2007.

[12] Chris Dunleavy David Brook Knowles, Kevin and Lianne Sallows. Atomic force microscopy. DoITPoMS, University of Cambridge, 10 2007.

[13] P. J. Zomer, M. H. D. Guimarães, J. C. Brant, N. Tombros, and B. J. van Wees. Fast pick up technique for high quality heterostructures of bilayer graphene and hexagonal boron nitride. *Applied Physics Letters*, 105(1):–, 2014.